Impact of Atomization Flow Structure and Turbulence on Droplet μ-explosions in the FSP Process

Malte F. B. Stodt [1,2], Johannes Kiefer[2,3], Udo Fritsching[1,3,4]

[1]Leibniz Institute for Materials Engineering IWT, Badgasteiner Str. 3, 28359 Bremen, Germany

[2]Technische Thermodynamik, Universität Bremen, Badgasteiner Str. 1, 28359 Bremen, Germany

[3]MAPEX Center for Materials and Processes, Universität Bremen, Am Fallturm 1, 28359 Bremen, Germany

[4]Faculty of Production Engineering, Universität Bremen, Bibliothekstr. 1, 28359 Bremen, Germany

*Corresponding author: m.stodt@iwt.uni-bremen.de

Keywords

flame spray pyrolysis, micro-explosions, spray combustion, drop dynamics, coaxial atomization

Abstract

In this work, the influence of atomization and flow conditions on the drop dynamics and evolution of drop size distributions in an nanoparticle producing spray flame are investigated experimentally by PDA. Especially, the formation of bimodal drop size distributions, that are product of severe μ-explosions, are a focus in this work. The flow conditions are chosen to cover the entire subsonic range of suitable operation conditions and are described using the relevant dimensionless numbers. To enable a proper comparison between different spray configurations, the gas-to-liquid mass ratio and, hence, the oxygen/fuel ratio were hold constant in order to identify the sole influence of flow conditions on the drop dynamics. It is found that all sprays present the formation of bimodal drop size distributions. Their evolution shows that high jet Reynolds numbers lead to narrower DSD and to a sharper sink between both probability peaks. Furthermore, size measurements of the final iron oxide particles showed that higher Reynolds numbers lead to smaller particle sizes.

Introduction

The field of multicomponent drop combustion in applications like automotive engines, rocket engines, marine propulsion systems, etc., has been extensively studied for several decades [1, 2, 3]. Still, huge saving potentials of fuels are considered to reduce the costs of operation and the CO_2-footprint of hydrocarbons. Applications of multicomponent drop combustion are invariably expanding, increasing their role on process efficiency and reduction of emissions. Since two decades, the flame spray pyrolysis (FSP) process enables the synthesis of metal oxides of mostly all metal elements of the periodic table [4, 5, 6]. This breakthrough further aroused the scientific interest in understanding the fundamentals of the physicochemical mechanisms (atomization, drop heating and evaporation) taking place during the lifetime of a burning drop. The development of specific process outlines for applications like battery design, drug delivery, and cell labelling among others is the key for tapping the full potential of tailored nanoparticles [5, 7]. Besides the nozzle geometry, the most relevant process parameter are the precursor and dispersion feed rate, as well as the choice of precursor and solvent combination [8, 9, 10, 11, 12]. Especially the latter is of great relevance as precursor solutions of high-enthalpy solvents and solvent mixtures of high boiling point difference have shown to present severe μ-explosions in isolated single drop experiments that are linked to the formation of homogeneous nanoparticles [13, 14, 15, 16]. In our prior works we could demonstrate that these μ-explosions also occur in high frequency in the spray flame of the SpraySyn burner during

FSP at standard conditions [17, 18]. It was found that μ-explosions lead to a conversion from unimodal drop size distributions (DSD) to bimodal DSDs. The dynamics of this phenomenon are still unclear. It is hypotesized that the onset of the formation of bimodal DSDs is mainly driven by the drop sizes that undergo μ-explosions which are mainly influenced by evaporation kinetics. The control of such dynamics is to be based on flow and mixing conditioning in the spray flame. Jüngst et al. also investigated the in-flight drop disruptions by image analysis of high-speed recordings and found similar drop sizes and similar puffing and μ-explosions for a similar precursor composition [19]. To study the influence of local flow conditions on the evolution of DSDs and nanoparticle size, phase-Doppler anemometry (PDA) experiments with a broad spectrum of jet Reynolds numbers are carried out that cover the entire range of possible operation conditions at subsonic flow velocities. The high complexity of FSP, however, challenges the comparison of varying operation conditions owing to a strong interplay within the whole process chain. Therefore, the oxidizer/fuel ratio of the spray was kept constant by setting the gas-to-liquid mass ratio (GLMR) constant throughout all experiments. This approach enables the investigation of the influence of the Reynolds number on the spray dynamics, the onset of μ-explosions and the final nanoparticle sizes.

Materials and Methods

Chemicals

All measurements are carried out using a 0.5 mol/L solution of iron nitrate nonahydrate (Merck kGaA) (FNT) dissolved in a mixture of ethanol (ethanol absolute, VWR Chemicals) and 2-ethylhexanoic acid (Sigma-Aldrich) with a volume ratio of 65:35. The chemicals were used as delivered. The solution is prepared dissolving FNT completely in the solvent mixture before filling up the measuring glass with the solvent mixture to the desired volume to reach a molarity of 0.5 mol/L. This is noteworthy since the density change from solid FNT to liquid FNT solutions is supposed to be significant.

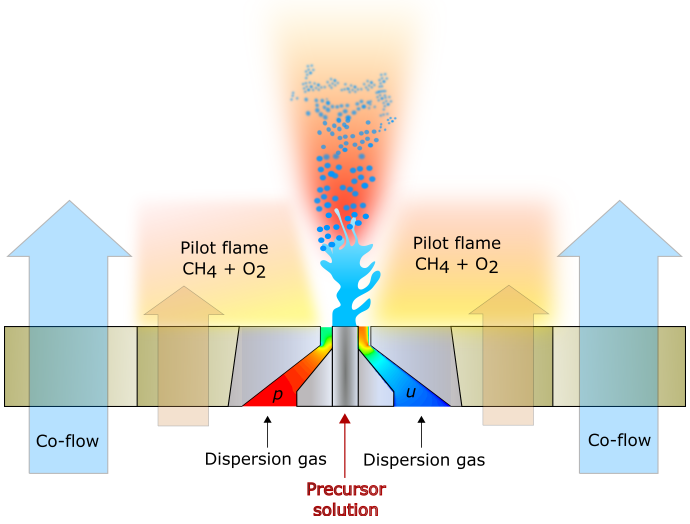

Figure 1. Sketch of the SpraySyn burner. The contours in the dispersion gas flow are representing the qualitative pressure (left side of the capillary) and gas velocity magnitudes (right side of the capillary).

Experimental Setup

The externally mixing twin-fluid nozzle SpraySyn is used on a bi-dimensional traversing system for measurements along the axial centre line of the spray flame. A schematic of the burner is shown in Fig. 1. The measurements are performed from 7.5 mm to 100 mm height above the

burner (HAB) with a step size of 2.5 mm. The precursor solution is introduced into the nozzle using a syringe pump (KD Scientific Gemini 88). For a detailed description of the materials and geometry the reader is referred to Schneider et al. [20]. All experiments were carried out under reactive conditions. The PDA setup used in this work is identical to that described in Stodt et al. [17]. The sample size is 40.000 for each measurement.
The nanoparticle's primary particle diameters are determined *via* Brunauer-Emmett-Teller (BET) analysis using a Quantachrome NOVA 4000e Autosorb system. The particles were degassed before the anylysis for 2h at 220 °. The isotherms were measured using nitrogen as adsorbent at 77 K. The specific surface area SSA and the bulk density ρ_{bulk} of the material (iron oxide ρ = 5250 kg m^{-3} [21]) are used to determine the equivalent primary particle diameter d_p by

$$d_p = \frac{6}{\rho_{\mathrm{bulk}}\,\mathrm{SSA}}. \tag{1}$$

Dimensionless Quantities
The relevant dimensionless numbers that are used to describe the flow conditions in the present spray flame are:

$$\mathrm{Re_g} = u_{\mathrm{g,exit}}\;\rho_{\mathrm{g,exit}}\;2s\;\eta_{\mathrm{g}}^{-1} \tag{2}$$

and

$$\mathrm{We_{aero}} = \rho_{\mathrm{g,exit}}\;(u_{\mathrm{g,exit}} - u_{\mathrm{l,exit}})^2\;d_{\mathrm{c}}\;\sigma^{-1}\;, \tag{3}$$

where $\mathrm{Re_g}$ and $\mathrm{We_{aero}}$ are the jet Reynolds and the aerodynamic Weber number, respectively. The exit gas velocity $u_{\mathrm{g,exit}}$ and density $\rho_{\mathrm{g,exit}}$ of the dispersion gas (O_2) are calculated considering the compressibility of the gas. The static pressure p is measured using a pressure gauge (Wika, 316SS) between the mass flow controller (Bronkhorst High-Tech B.V., Ruurlo, Netherlands) and the nozzle directly before the nozzle inlet. The density of the dispersion gas at the nozzle outlet conditions is calculated assuming an ideal gas by

$$\rho_{\mathrm{g,exit}} = \frac{p\;\widetilde{M}_{\mathrm{O_2}}}{R\,T} \tag{4}$$

with $\widetilde{M}_{\mathrm{O_2}}$, R and T being the molar mass of oxygen, the universal gas constant (R = 8.3145 J mol^{-1}K^{-1}) and temperature (T = 293.15 K), respectively. The momentum ratio M, the Mach-number Ma and the gas-to-liquid mass ratio (GLMR) are calculated using the following expressions

$$\mathrm{M} = \frac{\rho_{\mathrm{g,exit}}\;u_{\mathrm{g,exit}}^2}{\rho_{\mathrm{l,exit}}\;u_{\mathrm{l,exit}}^2} \tag{5}$$

$$\mathrm{Ma} = \frac{u_{\mathrm{g,exit}}}{c} \tag{6}$$

$$\mathrm{GLMR} = \frac{\dot{M}_g}{\dot{M}_l} \tag{7}$$

with c and $\dot{M}_{g/l}$ representing the speed of sound (c = 343 ms^{-1}) and the mass flow rate of the gas and liquid, respectively. The GLMR is constant throughout the entire experiments at GLMR = 7.9. The employed $\mathrm{Re_g}$ and $\mathrm{We_{aero}}$ numbers are listed in Tab. 1. The use of these dimensionless numbers further enables a comparison of the present spray flame with other types of spray flames, e.g. from the Thetis nozzle (ParteQ GmbH), Schlick nozzle or modified versions of the SpraySyn burner.

Table 1. Dimensionless quantities and static pressure p for the different operation conditions at the nozzle exit. The expression L/G represents the ratio of liquid (L) precursor flow rate in mL min^{-1} to dispersion gas (G) flow rate of O_2 in standard litres per minute (slm).

L/G	1.5/7.5	2/10	2.5/12.5	3/15	3.5/17.5	4/20
$\mathrm{Re_g}$ / -	5370	7160	8949	10739	12528	14320
$\mathrm{We_{aero}}$ / -	209	370	579	834	1135	1483
p / bar	0.15	0.21	0.32	0.48	0.61	0.78

Results and Discussion

Drop sizes and Velocities

The arithmetic mean drop size profiles for the different flow conditions along the axial centre line of the spray flames are displayed in Fig. 2a. While the mean drop sizes present similiar magnitudes in zones close to the burner, significant differences in the evolution of the mean sizes are observed in the spray far-field at HAB $\geq$ 30 mm. The sharp increase in mean drop sizes for the sprays with lower flow rates is mainly caused by the very fast evaporation of small drops and the presence of large drops that evaporate slowly (according to the d^2-law). The corresponding mean drop and gas velocities are shown in Fig. 2b. The gas velocities are estimated from tracer drops ($d_{\mathrm{D,T}} \leq 4$ µm) that accurately follow the gas flow (Stokes numbers $\mathrm{St} < 0.005$) [17]. As shown, the range of maximum flow velocity reaches from 100 ms^{-1} (L/G - 1.5/7.5) to 200 ms^{-1} (L/G - 4/20). All series present decreasing drop and gas velocities downstream owing to friction, jet expansion, and gravitational forces.

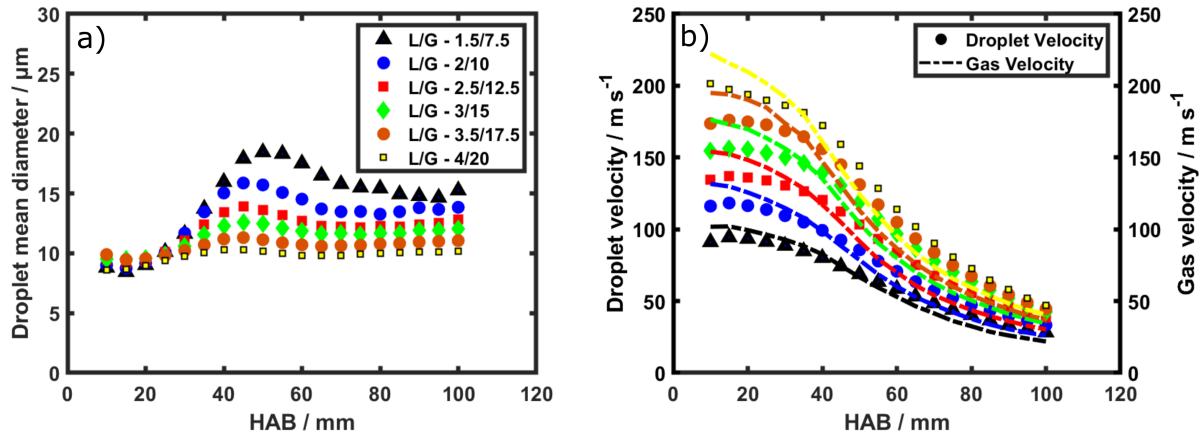

Figure 2. a) Evolution of the arithmetic mean diameter along the axial centre line of the spray; b) Axial drop and gas velocity profiles measured along the centre line.

Spray Flame Flow Conditions

In order to quantiatively describe the flow conditions and to identify the dominating forces acting in the spray flame the relevant dimensionless quantities are used. Figure 3a) displays the jet Reynolds number $\mathrm{Re_g}$ with the corresponding M ratios and shows a clear linear behavior which is expected. The inverse proportional relationship of $\mathrm{Re_g}$ and$\mathrm{M}$ results from the compressibility of the dispersion gas that lead to lower gas velocity increases compared to liquid velocity

increases. The present Ma numbers and M ratios over the whole range of dispersion gas flow rates is displayed in Fig. 3b). The Ma number covers a range of $0.50 \leq \mathrm{Ma} \leq 0.85$. Martins et al. experimentally measured the gas velocity closely above the nozzle exit by particle image velocimetry using similar process conditions [22] and determined Ma numbers of 0.3 This order of magnitude indicates the presence of gas compressibility effects. Compared to other FSP applications, the magnitudes of Ma numbers in the SpraySyn burner are relatively low as also transonic and supersonic Ma numbers have been applied in literature [23, 24, 25, 26, 27, 9]. The effect of compressibility effects further becomes visible in Fig. 3b). The M ratios behave inversely proportional to the dispersion gas flow rate as the static pressure increase leads to an compression of the dispersion gas. The increase in velocity of the gas-phase is therefore relatively lower than the increase in precursor velocity exiting the capillary. It is noteworthy that in case of an incompressible dispersion gas flow a constant M ratio with increasing flow rates at constant GLMR would be achieved. The magnitude of the M ratio of 10^2-10^3 and Ma numbers of 0.3 enable the formation of a fine spray with drops as small as 10 μm in average (see chapter *Drop sizes and Velocities*).

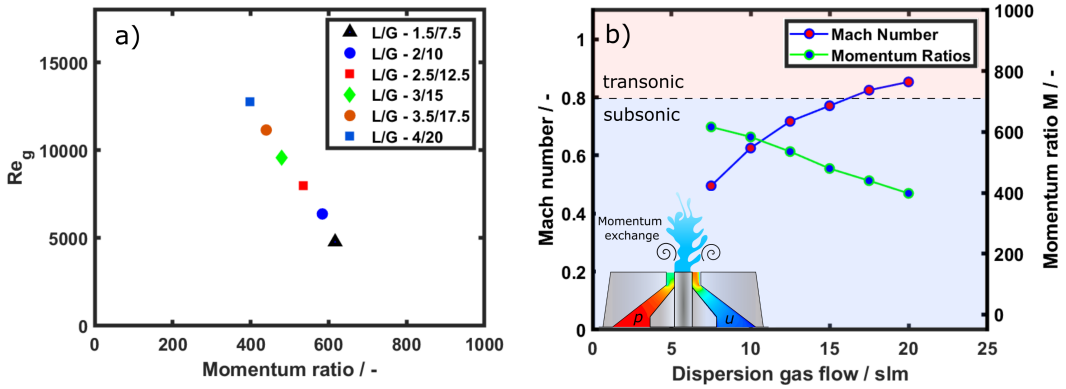

Figure 3. a) $\mathrm{Re_g}$ as a function of M ratio for the investigated precursor and dispersion gas flow rates; b) The Ma number and M ratio for the different dispersion gas flow rates. The inset illustrates the zone of momentum exchange between gas and liquid phase at the nozzle outlet.

Evolution of Drop Size Distributions

The DSD belongs to the most critical quantities in spray combustion. Especially their dynamics in space and time provide insights into ongoing evaporation and flow behavior. In presence of μ-explosions the change in shape and modality of size distributions further allow insights into the characteristics of μ-explosions. The evolution of the probability density histograms of DSDs along the axial centre line of the spray flame are shown in Fig. 4 for different precursor and dispersion gas flow rates. The evolution of DSDs are displayed with a resolution of 2.5 mm in HAB and 1 μm in drop size.

The configuration 2/10 shows the formation of a second peak at HAB = 30 mm which is driven towards drop sizes of $\approx$ 20-30 μm for HAB $\geq$ 60 mm. The increase in probability densities of larger drops along the spray is a common phenomenon that is attributed to the very fast evaporation of small drops. The sink in probability density between both peaks, however, is owing to the presence of μm-explosions that leads to the vanishing of certain drop sizes and the new formation of smaller drop sizes by the formation of secondary drops that are the outcome of μ-explosions [17]. The probability density of small drop size classes (3-10 μm) increases with increasing HAB for HAB $\geq$ 50 mm as a result of secondary drop formation. It is noteworthy that only secondary drops with a drop size of $d_\mathrm{D} \geq$ 0.5 μm are measured owing to experimental limitations. For larger flow rates, the formation of bimodal DSD is more pronounced and a sharp sink that increases with drop size and HAB becomes clear. The increasing drop size of the sink shows that the drop size of the drops undergoing μ-explosions increases with life time of the drops. A plausible explanation would be that the onset of μ-explosion is mainly driven by the

heating rate of the drop to reach bubble point temperature in the center region of the drop. This conclusion is consistent observations in the combustion of kerosene/water emulsions [28]. The significantly sharper formation of the sink might be caused by the enhanced convective mixing of reactants and oxygen in the flame that promotes a more effective combustion.

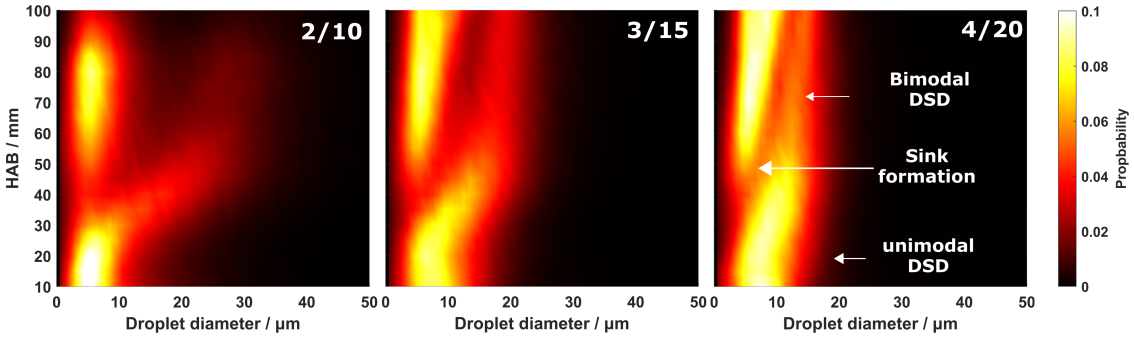

Figure 4. The evolution of DSDs along the axial centre line of the spray flame for different precursor and dispersion gas flow rates.

Influence of Flow Conditions on Nanoparticle Size

The resulting average primary particle sizes (BET diameter d_p) of the iron oxide nanoparticle product in dependence on the the jet Reynolds number Re_g and Momentum ratio M is shown in Fig. 5. The BET diameter d_p continuously increases with decreasing Re_g while the Momentum ratio increases. This is mainly driven by the degree of turbulence as strong velocity fluctuations and the mixing of reactants increase. It is suspected that these effects lead to shorter high-temperature residence times of the particles, thus, reducing the time scales for coagulation and sintering. This behaviour has been previously observed with varying dispersion gas flow rates at constant precursor feed rate in FSP [29, 30].

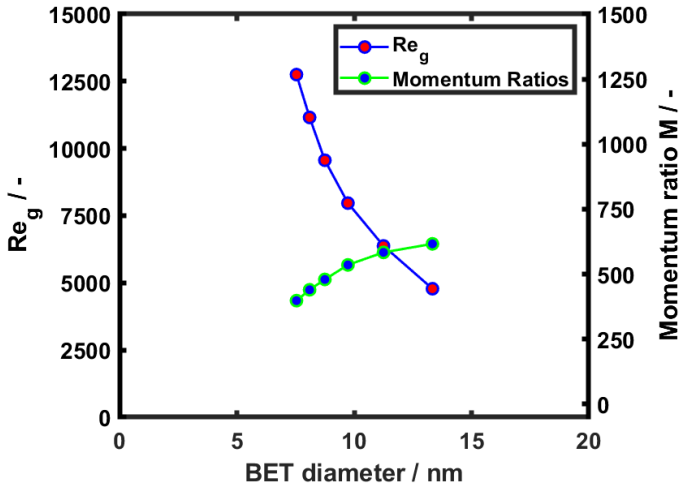

Figure 5. The primary particle diameter in dependence of the jet Reynolds number Re_g.

Conclusions

In this work the influence of flow conditions on the drop dynamics and the evolution of bimodal DSDs has been investigated for a broad range of operation conditions under constant GLMRs

and oxygen/fuel ratios. The spray formation is described by the relevant dimensionless quantities and the relation between the jet Reynolds number and Momentum ratio and the final primary particle are quantified for the SpraySyn burner. It is found that with an increasing jet Reynolds number the formation of bimodal DSDs, that are product of severe μ-explosions, is observed closer to the burner exit, thus, indicating an earlier onset of μ-explosions. Insights into the drop size evolution of disrupting drops have been gained by the evolution of the sink in the DSD between both peaks. The data show that the drop sizes of disrupting drops increase with HAB indicating that the phenomena in spray flames is mainly driven by the heating rate of the drops. Consequently, increasing the flow rates at constant GLMR in the subsonic range is a powerfull tool to control the nanoparticle diameter d_p without increasing the cost of production. The operation with Mach numbers close to unity are therefore favourable.

Acknowledgements
The financial support of this project through the German Research Foundation (DFG) within the priority program SPP 1980 SpraySyn under grants KI 1396/6-2 and FR 912/42-2 is gratefully acknowledged.

Nomenclature

c	speed of sound
d_c	inner capillary diameter
d_D	drop diameter
$d_\mathrm{D,T}$	tracer drop diameter
d_p	nanoparticle primary particle diameter
St	Stokes number
GLMR	gas-to-liquid mass ratio
HAB	height above the burner
M	Momentum ratio
$\tilde{M}$	molar mass
$\dot{M}$	mass flow rate
Ma	Mach number
p	pressure
R	universal gas constant
Re_g	jet Reynolds number
s	width of annular gap
SSA	specific surface area
T	gas phase temperature
$u_\mathrm{g,exit}$	gas velocity at nozzle outlet
$u_\mathrm{l,exit}$	liquid velocity at capillary outlet
u_D	droplet mean velocity
We_{aero}	aerodynamic Weber number
η_g	gas dynamic viscosity
ρ_{bulk}	bulk density
$\rho_{g,exit}$	gas density at nozzle outlet
$\rho_{l,exit}$	liquid density at capillary outlet
σ	surface tension

References

[1] G.T. Kalghatgi. *Proc. Combust. Inst.*, 35(1):101–115, 2015.
[2] A. Mazzetti, L. Merotto, and G. Pinarello. *Acta Astro.*, 126:286–297, 2016.

[3] P. Ni, X. Wang, and H. Li. *Fuel*, 279:118477, 2020.
[4] W.Y. Teoh, R. Amal, and L. Mädler. *Nanoscale*, 2(8):1324–1347, 2010.
[5] C. Schulz, T. Dreier, M. Fikri, and H. Wiggers. *Proc. of the Combust. Inst.*, 37(1):83–108, 2018.
[6] S. Pokhrel and L. Mädler. *Ener. Fuels*, 34(11):13209–13224, 2020.
[7] F. Meierhofer and U. Fritsching. *Ener. Fuels*, 35(7):5495–5537, 2021.
[8] F. Meierhofer, H. Li, M. Gockeln, R. Kun, T. Grieb, A. Rosenauer, U. Fritsching, J. Kiefer, J. Birkenstock, L. Mädler, and S. Pokhrel. *ACS Appl. Mater. Interfaces*, 9(43):37760–37777, 2017.
[9] F. Meierhofer, L. Mädler, and U. Fritsching. *AIChE J.*, 66(2), 2019.
[10] M.F.B Stodt, J. Kiefer, and U. Fritsching. *Exp. Fluids*, 60(8):125, 2019.
[11] M.F.B. Stodt, M. Gonchikzhapov, T. Kasper, U. Fritsching, and J. Kiefer. *Phys. Chem. Chem. Phys.*, 21(44):24793–24801, 2019.
[12] S. Angel, J. Neises, M. Dreyer, K. Friedel Ortega, M. Behrens, Y. Wang, H. Arandiyan, C. Schulz, and H. Wiggers. *AIChE J.*, 66(1):e16748, 2020.
[13] C.D. Rosebrock, N. Riefler, T. Wriedt, L. Mädler, and S.D. Tse. *AIChE J.*, 59(12):4553–4566, 2013.
[14] C.D. Rosebrock, T. Wriedt, L. Mädler, and K. Wegner. *AIChE J.*, 62(2):381–391, 2016.
[15] H Li, C.D. Rosebrock, N. Riefler, T. Wriedt, and L. Mädler. *Proc. of the Combust. Inst.*, 36(1):1011–1018, 2017.
[16] H. Li, C.D. Rosebrock, Y. Wu, T. Wriedt, and L. Mädler. *Proc. Combust. Inst.*, 37(1):1203–1211, 2019.
[17] M.F.B. Stodt, J. Kiefer, and U. Fritsching. *Atomization Sprays*, 30(11), 2020.
[18] M.F.B. Stodt, J. D. Groeneveld, L. Mädler, J. Kiefer, and U. Fritsching. *Combust. Flame*, 240:112043, 2022.
[19] N. Jüngst, G.J. Smallwood, and S.A. Kaiser. *Exp. Fluids*, 63(3):1–14, 2022.
[20] F. Schneider, S. Suleiman, J. Menser, E. Borukhovich, I. Wlokas, A. Kempf, H. Wiggers, and C. Schulz. *Rev. Scientific Instr.*, 90(8):085108, 2019.
[21] Gestis substance database, 2022.
[22] F.J.W.A Martins, J. Kirchmann, A. Kronenburg, and F. Beyrau. *Exp. Thermal Fluid Sci.*, p. 110052, 2020.
[23] M.C. Heine and S. E Pratsinis. *Ind. & Eng. Chem. Res.*, 44(16):6222–6232, 2005.
[24] M.C. Heine, L. Mädler, R. Jossen, and S.E. Pratsinis. *Combust. Flame*, 144(4):809–820, 2006.
[25] A.J. Gröhn, S.E. Pratsinis, and K. Wegner. *Chem. Eng. J.*, 191:491–502, 2012.
[26] H. Torabmostaedi, T. Zhang, P. Foot, S. Dembele, and C. Fernandez. *Powder Technol.*, 246:419–433, 2013.
[27] D. Noriler, C.D. Rosebrock, L. Madler, H.F. Meier, and U. Fritsching. *Atom. Sprays*, 24(6), 2014.
[28] S.S. Sazhin, E. Shchepakina, V.A. Sobolev, D.V. Antonov, and P.A. Strizhak. *Int. J. Heat Mass Transf-*, 184:122210, 2022.
[29] H.K. Kammler, L. Mädler, and S.E. Pratsinis. *Chem. Eng. & Technol.*, 24(6):583–596, 2001.
[30] S. Angel, F. Schneider, S. Apazeller, W. Kaziur-Cegla, T.C. Schmidt, C. Schulz, and H. Wiggers. *Proc. Combust. Inst.*, 38(1):1279–1287, 2021.